Systemic chemotherapy decreases brain glucose metabolism

ANNALS of Clinical and Translational Neurology
Open Access
ANA American Neurological Association since 1875

RESEARCH ARTICLE

Systemic chemotherapy decreases brain glucose metabolism

Laura L. Horky[1], Victor H. Gerbaudo[1], Alexander Zaitsev[1], Wen Plesniak[1], Jon Hainer[1], Usha Govindarajulu[1], Ron Kikinis[1] & Jörg Dietrich[2]

[1]Division of Nuclear Medicine, Department of Radiology, Brigham and Women's Hospital, Harvard Medical School, 75 Francis Street, Boston, Massachusetts, 02115

[2]Division of Neuro-Oncology, Department of Neurology, Massachusetts General Hospital Cancer Center and Center for Regenerative Medicine, Harvard Medical School, 55 Fruit Street, Yawkey 9E, Boston, Massachusetts, 02114

Correspondence
Jörg Dietrich, Department of Neurology, Harvard Medical School, 55 Fruit Street, Yawkey 9E, Boston, MA 02114. Tel: 617-724-8770; Fax: 617-724-8769; E-mail: Dietrich.Jorg@mgh.harvard.edu

Funding Information
This work was supported by the National Institutes of Health (NIH) (P41 EB015898; P41 RR013218; U54 EB005149; to R. K., A. Z., and W. P). J. Dietrich is a recipient of the American Academy of Neurology (AAN) Clinical Research Training Fellowship (CRTF). This work has also been supported by the Clinical Investigator Program (CITP) at Beth Israel Deaconess Medical Center, Harvard Medical School (to J. D.), the American Cancer Society (to J. D.), and internal funds from the Department of Radiology at BWH (to L. H.).

Received: 21 April 2014; Revised: 27 July 2014; Accepted: 18 August 2014

Annals of Clinical and Translational Neurology **2014; 1(10): 788–798**

doi: 10.1002/acn3.121

Abstract

Objective: Cancer patients may experience neurologic adverse effects, such as alterations in neurocognitive function, as a consequence of chemotherapy. The mechanisms underlying such neurotoxic syndromes remain poorly understood. We here describe the temporal and regional effects of systemically administered platinum-based chemotherapy on glucose metabolism in the brain of cancer patients. **Methods**: Using sequential FDG-PET/CT imaging prior to and after administration of chemotherapy, we retrospectively characterized the effects of intravenously administered chemotherapy on brain glucose metabolism in a total of 24 brain regions in a homogenous cohort of 10 patients with newly diagnosed non-small-cell lung cancer. **Results**: Significant alterations of glucose metabolism were found in response to chemotherapy in all gray matter structures, including cortical structures, deep nuclei, hippocampi, and cerebellum. Metabolic changes were also notable in frontotemporal white matter (WM) network systems, including the corpus callosum, subcortical, and periventricular WM tracts. **Interpretation**: Our data demonstrate a decrease in glucose metabolism in both gray and white matter structures associated with chemotherapy. Among the affected regions are those relevant to the maintenance of brain plasticity and global neurologic function. This study potentially offers novel insights into the spatial and temporal effects of systemic chemotherapy on brain metabolism in cancer patients.

Introduction

Treatment of cancer with chemotherapy can be associated with a wide range of adverse effects as a consequence of toxicity to multiple organ systems. Dose-limiting toxicity of chemotherapy frequently affects tissues that harbor rapidly dividing cell populations, such as the gastrointestinal tract and the hematopoietic system. While the central nervous system (CNS) traditionally has been considered much less vulnerable to the effects of chemotherapy, recent clinical and experimental studies have revealed that varying degrees of CNS toxicity might be more prevalent than previously anticipated.

CNS toxicity from chemotherapy may include acute, subacute, and delayed effects, and in some patients may result in generalized neurological decline with cognitive impairment, infrequently coupled with radiographic findings of brain atrophy and white matter (WM) abnormalities.[1] Cognitive impairment as a late complication of chemotherapy and radiation has long been observed in pediatric cancer patients.[2–6] Increasing survival rates of adult cancer patients and analysis of survivors in longitudinal studies

using neuropsychological testing have revealed growing evidence that chemotherapy can be associated with long-term alteration of cognitive function.[7–21]

Noteworthy, there are currently no standardized diagnostic tests available to monitor patients for potential neurotoxicity, or to identify those individuals at risk. Although neuroimaging studies have invariably demonstrated nonspecific abnormalities, several recent prospective imaging studies with magnetic resonance imaging (MRI), functional MRI (fMRI), and positron emission tomography (PET) have supported the notion that structural and functional brain changes occur in a significant number of patients.[22–25]

Neuroimaging and cognitive effects of chemotherapy have been most widely studied in breast cancer patients.[26] Structural MRI studies in breast cancer patients treated with systemic chemotherapy have revealed decreased regional volumes of gray and WM structures, including prefrontal and parahippocampal regions.[27] Consistent with these early studies, subsequent MRI studies identified reductions in overall brain volume,[28] and more specifically in frontal, temporal, and cerebellar cortices in breast cancer patients examined longitudinally prior to and after chemotherapy.[29] MRI studies using diffusion tensor imaging (DTI) identified disseminated WM damage secondary to systemic chemotherapy in breast cancer patients.[22,25,30,31] Functional imaging studies with fMRI have suggested that regionally altered brain function in breast cancer patients treated with chemotherapy correlates with cognitive impairment and diminished executive function.[32–34] Very little is known of the impact of chemotherapy on glucose metabolism in the brain. Using [O-15] H_2O and [F-18] fluorodeoxyglucose (FDG) PET in a cohort of breast cancer survivors, treated with chemotherapy 5–10 years prior, the authors identified chronic gray matter (GM) alterations in fronto-cortical, cerebellar, and basal ganglia activity.[35] Resting glucose metabolism in inferior-frontal brain regions correlated with impaired short-term memory function in the same patient cohort.[35] A subsequent FDG-PET/CT brain imaging study found a correlation between circulating pro-inflammatory cytokines, cognitive complaints, and regionally impaired glucose metabolism in the medial prefrontal cortex and anterior temporal cortex in a cohort of breast cancer survivors monitored over 1 year[36]; however, imaging data prior to administration of chemotherapy were not obtained in both studies.

Insights into potential mechanisms of neurotoxicity following chemotherapy have come from preclinical studies.[37] We have previously shown both in vitro and in vivo that diverse classes of conventional chemotherapeutic agents, such as antimetabolites and alkylating agents may be harmful to neural progenitor cell populations relevant for the maintenance of normal brain function, WM integrity, gliogenesis, and neurogenesis.[38–42] In particular, platinum compounds and other alkylating agents can be harmful to the CNS with potentially long-lasting effects on neural repair and brain plasticity.[38]

Using FDG-PET in combination with an advanced imaging analysis technology specifically developed for this study, we here describe the temporal and regional effects of platinum-based chemotherapy on resting glucose metabolism in the brain of a homogenous cohort of non-small-cell lung cancer (NSCLC) patients followed longitudinally pre- and post treatment. We retrospectively analyzed brain regions of interest (ROI) in GM, WM, and germinal zones, thought to be relevant for the maintenance of brain plasticity in the adult CNS.

Patients and Methods

Patient selection criteria

We searched the Brigham & Women's Hospital (BWH) Nuclear Medicine clinical database between 2005 and 2012 for patients who underwent serial FDG-PET scans as part of cancer staging at both baseline and follow-up after receiving chemotherapy.

Based on our preclinical studies demonstrating preferential neurotoxic effects on brain plasticity with platinum compounds and other alkylating agents, and in order to identify a homogenous patient population suitable for the objective of this imaging study, we focused our search on patients aged 18, or older, with newly diagnosed non-small-cell lung cancer receiving a platinum-based treatment protocol as part of their initial management. Importantly, any patient with active or previous neurologic disease or with a history of prior chemotherapy (for any cancer or condition) was excluded. Patients with evidence of brain metastasis were also excluded from this study. Patients were required to have a normal renal and liver function both pre- and post chemotherapy. In addition, patients taking any medications that potentially could influence brain function and brain metabolism (e.g., benzodiazepines, opiates, narcotics, antidepressants, and steroids) were not eligible for this study.

We identified a total of 541 patients who underwent PET imaging as part of their staging studies for non-small-cell lung cancer between 2005 and 2012; however, only 156 patients underwent multiple longitudinal PET studies. Of these, 146 patients were excluded from the study, since they did not meet the strict eligibility criteria noted above (e.g., no prior chemotherapy, history of neurological or psychiatric disease, metastatic disease to the brain, longitudinal PET images not obtained at the

Brigham and Women's Hospital, use of medications with potential effect on brain function, etc.).

This retrospective study was reviewed and approved by the institutional review board (IRB). All patients had clinically scheduled whole-body staging FDG-PET/CT studies prior to initiation of cancer therapy. The BWH clinical whole-body PET/CT protocol includes *whole-brain imaging*, creating a unique database for longitudinal studies, with a baseline scan prior to treatment and at least one follow-up scan after starting chemotherapy. The design of this study therefore provided the unique opportunity to use each patient's baseline imaging as a control for subsequent scans.

Clinical imaging protocol

Patients were injected intravenously with ^{18}F-FDG at a standard dose of 20 mCi for whole-body imaging in two-dimensional mode. PET/CT images were acquired on a Discovery ST PET/CT scanner (General Electric, Milwaukee, WI) at 45–60 min after tracer injection. The unenhanced CT scan was performed first using the following parameters: 140 kVp, 15 mA, 30 cm DFOV, pitch 0.531:1, 32 slice helical, 3.75 mm slice thickness, and 10.62 mm/rotation. The CT data were reconstructed using a filtered back projection algorithm and a 128 × 128 matrix, ramp cutoff of 5.8 mm, with 30 cm trans-axial field of view. The PET data were reconstructed using an iterative ordered subsets expectation maximization (OSEM) algorithm (28 subsets, two iterations), a standard *z* axis filter, 3.74 mm post filter, a 128 × 128 matrix, and a DFOV 43.6 mm. Random coincidences were estimated using single crystal event rates.

Plasma glucose concentration was measured prior to each scan by finger stick. All patients were instructed to take nothing by mouth but water for at least 4–6 h prior to the study. Blood glucose levels were not statistically different ($P = 0.34$; paired *t*-test) between baseline (mean of 106.2 ± 4.6 mg/dL [SEM]; 95% CI: 95.7–116.8 mg/dL) and at time of follow-up PET scans post chemotherapy (mean of 114.0 ± 9.5 mg/dL [SEM]; 95% CI: 92.1–135.9 mg/dL). This variation is similar to the variation expected with time in normal individuals. The lumped constant (LC), defined as the conversion factor between the net uptake of FDG and glucose,[43] was assumed to be constant over time, given the lack of evidence that LC values change in the setting of chemotherapy. All subjects rested quietly during the 45- to 60-min FDG uptake period with eyes open in a dark room per standard clinical protocol.

Image processing

We used 3DSlicer (www.slicer.org)[44] and BRAINSfit (http://hdl.handle.net/1926/1291), an innovative open-source imaging analysis technology, for image processing. The technology was modified for use in brain PET imaging. First, whole-body PET/CT images were converted from DICOM format to Nearly Raw Raster Data (NRRD) format, 3DSlicer's native format for imaging manipulation and processing. The whole-body PET and CT images were cropped to isolate the brain image data sets. Two sets of PET and CT brain images were coregistered to each other: one set performed at baseline prior to initiating chemotherapy and the other after chemotherapy. This coregistration process resulted in matching PET and CT axial images, in which corresponding voxels or ROI drawn in any of the image matrixes could be accurately mapped to the same anatomic location within each data set. Whenever available, MR images were also processed and coregistered to PET and CT to assist with the identification of anatomic structures.

ROI

Using coregistered images, a total of 24 brain ROI, including 13 GM, seven WM, and four germinal zone regions (subventricular zone and medial temporal lobe/hippocampus), were contoured on each subject's scan, as summarized in Table 1. ROI were placed manually (using 3DSlicer) by a blinded co-Investigator (L. H.). The size of each ROI varied according to the size of the structure (smaller for small structures such as hippocampus and

Table 1. Regions of interest (ROI) analyzed prior to and after chemotherapy.

Gray matter structures ($n = 13$)	White matter structures ($n = 7$)	Germinal zones ($n = 4$)
Caudate head (right/left)	Paraventricular white matter (right/left)	Medial temporal lobe/hippocampus (right/left)
Thalamus (right/left)	Corpus callosum (genu)	Subventricular zone (right/left)
Frontal cortex (right/left)	Corpus callosum (splenium)	
Parietal cortex (right/left)	Subcortical white matter (right/left)	
Cerebellar cortex (right/left)	Cerebellar white matter (right)	
Posterior cingulate gyrus		
Olfactory gyrus (right/left)		

larger for structures such as posterior cingulate gyrus and frontal GM). In each case, each ROI was placed on the axial slice that best demonstrated the region. Since PET scans were coregistered to one another, this allowed for duplication of ROI to corresponding areas of the brain on each modality at each time point. This method optimizes reproducibility in ROI placement. An example of the ROI placement identified on PET and corresponding MR images is shown in Figure 1. From the ROI, SUV_{mean} (standardized uptake $value_{mean}$) and SUV_{max} were obtained. SUV_{mean} quantifies the average SUV in the region of interest. SUV_{max} defines the voxel of highest metabolism within the entire region. SUVs were analyzed longitudinally over time for each patient in all ROI, to include a pre- and post-chemotherapy data set.

Statistical analysis

Results were expressed as the mean and its corresponding standard error (SE), and 95% confidence intervals (CI). Right versus left comparisons of metabolic activity in cerebral regions as a function of treatment were performed within each patient using the paired *t*-test (two-tailed). $P < 0.05$ was used to define statistical significance. In addition, we used multivariate analysis of variance (MANOVA) to determine possible differences among brain regions within GM, WM, and germinal zones. $P < 0.05$ was used to define statistical significance.

Results

Patient characteristics and study design

A homogenous group of 10 adult subjects with newly diagnosed NSCLC were evaluated in this study (mean age 63, range 48–78, including seven males and three females). All patients received initial treatment with conventional chemotherapy consisting of a platinum-based regimen, as summarized in Table 2. In addition, two subjects subsequently also received Pemetrexed (Alimta), a folate antagonist, and three subjects received additional chemotherapy with bevacizumab (Avastin), a humanized monoclonal antibody directed against vascular endothelial growth factor (VEGF). Baseline brain imaging with FDG-PET/CT was performed prior to initiating chemotherapy. Restaging studies were performed after a mean of four cycles of chemotherapy (range 1–7 cycles), corresponding to a mean time interval of 181 days or 6 months (range 88–402 days) between baseline and follow-up scans. Patients were off active chemotherapy at the time of follow-up PET/CT for a mean of 11 days (range 2–28 days).

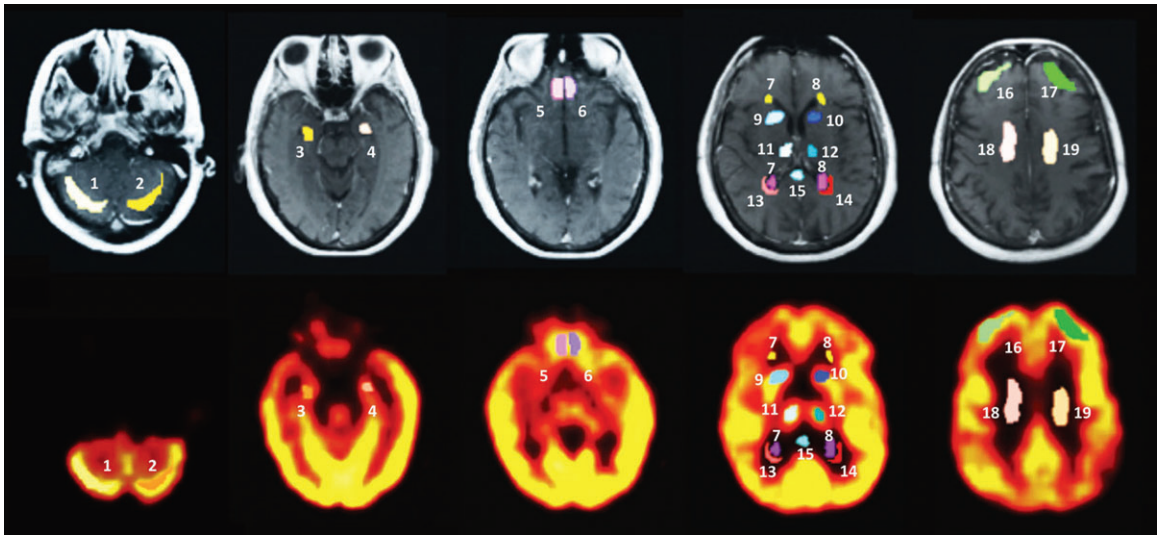

Figure 1. Regions of interest (ROI) placement on PET and corresponding magnetic resonance images. The figure shows an example of the ROI placement in gray and white matter regions and in germinal zones on magnetic resonance imaging (upper panel) and coregistration with corresponding PET scans (lower panel). From a total of 24 regions both SUV_{mean} and SUV_{max} were obtained. SUVs were analyzed longitudinally over time for each patient in all ROI, to include a pre- and postchemotherapy data set. (1,2): right and left cerebellar cortex; (3,4): right and left medial temporal lobe and hippocampus; (5,6): right and left orbitofrontal cortex/olfactory gyrus; (7,8): right and left anterior and posterior subventricular zone; (9,10): right and left caudate nucleus; (11,12): right and left thalamus; (13,14): right and left periventricular white matter; (15): corpus callosum (splenium); (16,17): right and left frontal cortex; (18,19): right and left subcortical white matter; Not shown in this representative image are: right and left parietal cortex, corpus callosum (genu), posterior cingulate, and cerebellar white matter. PET, positron emission tomography; SUV, standardized uptake value.

Table 2. Demographic factors, clinical characteristics, chemotherapy regimen, response assessment, and time intervals of imaging follow-up of patients analyzed with serial PET/CT studies.

ID	Sex	Age	Pathology	Staging	Chemotherapy	No. of cycles	Response to therapy	Time (baseline – follow-up imaging) (in days)	Time (end of chemotherapy to follow-up imaging) (in days)	Memory problems and/or depression[1]
1	M	59	NSCLC	IIIb	Carboplatin/taxol[2]	3	PR			
					Carboplatin/ gemcitabine/avastin	3	PR	230	5	?
2	F	64	NSCLC	IIIb	Cisplatin/etoposide	1	SD	111	11	?
3	M	48	NSCLC	IIIb	Carboplatin/taxol	3	PR	81	5	?
4	M	64	NSCLC	IIIb	Cisplatin/gemcitabine	3	PD	311	28	Yes
					Cisplatin/navelbine	4	SD			
5	M	71	NSCLC	IIIa	Carboplatin/taxol	4	PD			
					Alimta (pemetrexed)	2	SD	402	10	Yes
6	M	63	NSCLC	IIIb	Carboplatin/taxol	4	PD	88	10	Yes
7	F	74	NSCLC	IIIa	Cisplatin/etoposide	2	PR	132	22	Yes
8	M	58	NSCLC	IIIb	Carboplatin/taxol/ avastin	2	PD			
					Alimta	2	PD	142	2	?
9	M	78	NSCLC	IIIb	Carboplatin/taxol	4	PR	171	13	Yes
10	F	46	NSCLC	IV	Carboplatin/taxol/ avastin	4	PD	140	8	Yes

PR, partial response; SD, stable disease; PD, progressive disease.

[1]Memory disturbance and mood alterations were assessed based on subjective patient reports and evidence in the patient's interval history.

[2]Patient had a partial response, however, developed intolerance/allergy to taxol; therefore, treatment was changed to carboplatin/gemcitabine/avastin.

Significant decrease in resting brain glucose metabolism in GM structures following systemic platinum-based chemotherapy

Significant decreases in resting brain glucose metabolism between baseline and follow-up imaging were identified in all 13 GM structures in response to platinum-based chemotherapy (Tables 3 and 4). Using SUV_{max} criteria, reductions of up to 20% (SE = 3.0%; 95% CI, 14–26%) were observed in resting brain glucose metabolism in all GM structures, including bilateral frontal and parietal cortices, cerebellum, deep nuclei, and posterior cingulate gyrus (Table 3). Most profoundly affected were the right frontal cortex (decrease by 24.0% [SE = 6.0%], [95% CI, 11–38%]; $P = 0.004$), left frontal cortex (decrease by 23.0% [SE = 5.4%], [95% CI, 11–35%]; $P = 0.004$), and the bilateral olfactory gyri (decrease by 22.0% [SE = 5.0%], [95% CI, 12–33%]; $P = 0.002$). Comparisons of SUV_{mean} pre- and post chemotherapy also demonstrated similar decreases in resting brain glucose metabolism, most notably in the right frontal cortex (decrease by 26.0% [SE = 6.0%], [95% CI, 13–40%]; $P = 0.004$), left frontal cortex (decrease by 23.0% [SE = 6%], [95% CI, 10–35%]; $P = 0.004$), and bilateral olfactory gyri (decrease by 23.0% [SE = 4%], [95% CI, 14–33%]; $P = 0.001$) (Table 4). The mean overall reduction in SUV_{mean} values in all 13 GM ROI was 22.0% (SE = 1.5%), (95% CI, 19–25%).

Differential impact on WM structures following platinum chemotherapy

Although an overall decrease of 10% in SUV_{max} and SUV_{mean} was seen in all WM structures (Tables 3 and 4),

Table 3. Max SUV of regions of interest.

Region of Interest	Max SUV (SE) baseline	95% CI baseline	Max SUV (SE) follow-up	95% CI follow-up	*P*-value baseline vs. follow-up	Avg. % change baseline vs. follow-up	95% CI
Gray matter							
Right caudate head	9.85 (1.08)	7.4–12.3	8.23 (1.10)	5.8–10.7	0.017	−17.0	−0.32 to −0.03
Left caudate head	9.54 (0.83)	7.7–11.4	8.05 (1.10)	5.6–10.5	0.021	−17.0	−0.30 to −0.05
Right thalamus	10.26 (0.99)	8.4–12.1	8.10 (0.99)	5.9–10.3	0.014	−21.0	−0.36 to −0.06
Left thalamus	10.34 (0.83)	8.5–12.2	8.24 (0.95)	6.1–10.4	0.012	−20.0	−0.34 to −0.06
Right frontal cortex	12.05 (0.96)	9.9–14.2	9.07 (1.01)	6.8–11.4	0.004	−24.0	−0.38 to −0.11
Left frontal cortex	11.35 (0.97)	9.1–13.5	8.72 (0.96)	6.5–10.9	0.004	−23.0	−0.35 to −0.11
Right parietal cortex	11.24 (0.92)	9.2–13.3	8.92 (0.99)	6.7–11.2	0.014	−20.0	−0.36 to −0.04
Left parietal cortex	10.82 (1.03)	8.5–13.1	8.55 (1.00)	6.3–10.8	0.015	−20.0	−0.35 to −0.05
Right cerebellum	9.80 (0.84)	7.9–11.7	8.02 (0.80)	6.2–9.8	0.020	−17.0	−0.31 to −0.03
Left cerebellum	9.75 (0.85)	7.8–11.7	7.86 (0.76)	6.1–9.6	0.021	−18.0	−0.32 to −0.04
Post cingulate gyrus	11.50 (1.06)	9.1–13.9	9.11 (1.04)	6.7–11.5	0.006	−20.0	−0.34 to −0.07
Right olfactory gyrus	9.92 (0.67)	8.4–11.4	7.75 (0.70)	6.2–9.3	0.001	−22.0	−0.33 to −0.11
Left olfactory gyrus	9.93 (0.67)	8.4–11.4	7.77 (0.76)	6.1–9.5	0.002	−22.0	−0.34 to −0.07
White matter							
Right paraventricular WM	5.53 (0.90)	4.9–6.2	4.80 (1.00)	4.1–5.5	0.007	−13.0	−0.22 to −0.05
Left paraventricular WM	5.42 (1.05)	4.6–6.2	4.69 (1.02)	4.0–5.4	0.120 (n.s.)	−11.0	−0.29 to −0.08
Corpus callosum	4.97 (1.15)	4.2–5.8	4.15 (1.20)	3.3–5.8	0.004	−17.0	−0.26 to −0.07
Right subcortical WM	4.93 (2.92)	2.8–7.0	4.53 (1.43)	3.5–5.5	0.550 (n.s.)	0.0	−0.19 to +0.18
Left subcortical WM	5.08 (3.33)	2.7–7.5	4.16 (1.45)	3.1–5.2	0.212 (n.s.)	−10.0	−0.26 to +0.05
Posterior corpus callosum	7.56 (5.80)	3.4–11.7	6.04 (4.17)	3.1–9.0	0.059 (n.s.)	−13.0	−0.30 to +0.11
Cerebellar WM	8.87 (5.31)	5.1–12.7	7.36 (3.68)	4.7–10.0	0.129 (n.s.)	−9.0	−0.29 to −0.08
Germinal zone							
Right hippocampus	6.90 (1.55)	5.8–8.0	6.31 (2.08)	4.8–7.8	0.150 (n.s.)	−9.0	−0.21 to +0.03
Left hippocampus	7.00 (1.91)	5.6–8.4	6.24 (1.93)	4.9–7.6	0.106 (n.s.)	−9.0	−0.23 to +0.04
Right SVZ	5.35 (1.45)	4.3–6.4	4.62 (1.32)	3.7–5.6	0.009	−13.0	−0.23 to −0.03
Left SVZ	4.60 (1.21)	3.7–5.5	4.23 (1.43)	3.2–5.3	0.121 (n.s.)	−9.0	−0.20 to +0.02
All gray matter ROI	10.49 (0.23)	10.00–10.98	8.34 (0.25)	7.84–8.84	0.0001	−20.0	−0.14 to −0.26
All white matter ROI	6.05 (0.43)	5.19–6.91	5.10 (0.30)	4.51–5.70	0.0001	−10.0	−0.05 to −0.16
Germinal zones	5.96 (0.29)	5.38–6.54	5.33 (0.30)	4.73–5.93	0.0002	−10.0	−0.05 to −0.15

SUV, standardized uptake value; WM, white matter; SVZ, subventricular zone; ROI, regions of interest; SE, standard error; CI, confidence interval; n.s., not significant.

Table 4. Mean SUV of regions of interest.

Region of interest	Mean SUV (SE) baseline	95% CI baseline	Mean SUV (SE) follow-up	95% CI follow-up	*P*-value baseline vs. follow-up	Avg. % change baseline vs. follow-up	95% CI
Gray matter							
Right caudate head	8.35 (0.74)	6.7–10.0	6.78 (2.60)	4.9–8.6	0.008	−20.0	−0.33 to −0.07
Left caudate head	8.38 (0.70)	6.8–10.0	6.77 (2.57)	4.9–8.6	0.004	−20.0	−0.32 to −0.08
Right thalamus	9.02 (0.81)	7.4–10.6	7.00 (2.57)	5.2–8.8	0.010	−22.0	−0.36 to −0.08
Left thalamus	9.07 (0.71)	7.5–10.7	7.19 (2.50)	5.4–9.0	0.012	−20.0	−0.33 to −0.07
Right frontal cortex	10.33 (0.78)	8.6–12.1	7.55 (2.52)	5.7–9.4	0.004	−26.0	−0.40 to −0.10
Left frontal cortex	9.94 (0.80)	7.8–11.4	7.41 (2.50)	5.6–9.2	0.004	−23.0	−0.36 to −0.07
Right parietal cortex	9.61 (0.80)	7.8–11.4	7.60 (2.57)	5.8–9.4	0.014	−20.0	−0.35 to −0.05
Left parietal cortex	9.27 (0.87)	7.3–11.2	7.22 (2.46)	5.4–9.0	0.008	−21.0	−0.34 to −0.08
Right cerebellum	8.35 (0.61)	7.0–9.7	6.81 (2.03)	5.4–8.3	0.016	−18.0	−0.32 to −0.04
Left cerebellum	8.40 (0.67)	6.9–9.9	6.80 (1.92)	5.4–78.2	0.010	−18.0	−0.30 to −0.06
Post cingulate gyrus	10.19 (0.89)	8.2–12.2	8.14 (2.65)	6.2–10.0	0.008	−19.0	−0.33 to −0.06
Right olfactory gyrus	8.94 (0.62)	7.5–10.3	6.82 (1.86)	5.5–8.2	0.001	−23.0	−0.33 to −0.14
Left olfactory gyrus	9.02 (0.63)	7.6–10.4	6.88 (1.96)	5.5–8.3	0.001	−23.0	−0.33 to −0.14
White matter							
Right paraventricular WM	4.17 (0.22)	3.7–4.7	3.63 (0.50)	3.3–4.0	0.018	−12.0	−0.22 to −0.008
Left paraventricular WM	3.69 (0.24)	3.2–4.2	3.26 (0.60)	2.8–3.7	0.063 (n.s.)	−10.0	–0.23 to +0.04
Corpus callosum (genu)	3.83 (0.18)	3.4–4.2	3.29 (0.82)	2.7–4.2	0.018	−14.0	–0.26 to −0.04
Right subcortical WM	3.71 (0.40)	2.8–4.6	3.38 (.078)	2.8–3.9	0.294 (n.s.)	−6.0	–0.20 to +0.09
Left subcortical WM	3.69 (0.42)	2.7–4.6	3.31 (0.75)	2.8–3.8	0.215 (n.s.)	−7.0	–0.20 to +0.06
Corpus callosum (splenium)	4.62 (0.18)	3.0–6.3	4.01 (1.74)	2.8–5.3	0.098 (n.s.)	−9.0	–0.21 to +0.04
Cerebellar WM	6.00 (0.51)	4.9–7.1	5.32 (1.42)	4.3–6.3	0.178 (n.s.)	−9.0	–0.27 to +0.09
Germinal Zone							
Right hippocampus	6.40 (0.49)	5.3–7.5	5.71 (1.87)	4.4–7.0	0.081 (n.s.)	−11.0	–0.23 to +0.01
Left hippocampus	6.43 (0.56)	5.2–7.7	5.77 (1.79)	4.5–7.1	0.065 (n.s.)	−9.0	–0.21 to +0.02
Right SVZ	4.53 (0.38)	3.7–5.4	3.94 1.01)	3.2–4.7	0.036	−12.0	–0.24 to +0.002
Left SVZ	4.04 (0.34)	3.3–4.8	3.57 (1.08)	2.8–4.3	0.043	−11.0	–0.23 to +0.004
All gray matter ROI	9.12 (0.20)	8.72–9.52	7.04 (0.19)	6.7–7.41	0.00003	−22.0	−0.25 to −0.19
All white matter ROI	4.24 (0.18)	3.89–4.60	3.74 (0.14)	3.5–4.0	0.00001	−9.0	−0.14 to −0.05
Germinal zones	5.35 (0.28)	4.79–5.91	4.75 (0.28)	4.19–5.31	0.00007	−11.0	−0.16 to −0.06

SUV, standardized uptake value; WM, white matter; SVZ, subventricular zone; ROI, regions of interest; SE, standard error; CI, confidence interval; n.s., not significant.

a significant decrease in SUV_{max} was only seen in two of seven structures: the right paraventricular WM (decrease by 13% [SE = 4%], [95% CI, 5–22%]; $P = 0.007$) and the genu of the corpus callosum (decrease by 17% [SE = 4%], [95% CI, 7–26%]; $P = 0.004$) (Table 3). Consistent with these findings, *significant* reductions in SUV_{mean} were also seen in the right paraventricular WM (decrease by 12% [SE = 5%], [95% CI, 0.8–22%]; $P = 0.018$) and the genu of the corpus callosum (decrease by 14% [SE = 5%], [95% CI, 3–26%]; $P = 0.018$) (Table 4).

Platinum-based chemotherapy decreases glucose metabolism in germinal zones of the CNS

To assess the impact of chemotherapy on germinal zones of the adult CNS, defined as regions of the brain that harbor neural progenitor cell and stem cell populations with the ability to respond to injury and to differentiate into neuronal and glial lineages, we analyzed changes in glucose metabolism in bilateral subventricular zones (SVZ) and bilateral hippocampi in the medial temporal lobes. Significant reductions in SUV_{max} were noted in the right subventricular zone (decrease by 13% [SE = 4%], [95% CI, 3–23%]; $P = 0.009$) and in the mean glucose metabolism both in the right subventricular zone (decrease by 12% [SE = 5%], [95% CI, 0.2–24%]; $P = 0.036$) and in the left subventricular zone (decrease by 11.0% [SE = 5%], [95% CI, 0.4–23%]; $P = 0.043$). While reduction of hippocampal glucose metabolism was also noted in terms of both SUV_{mean} and SUV_{max}, these changes did not reach significance. However, overall reductions across all germinal zone structures reached 11% in SUV_{mean} and 10% in SUV_{max}.

Collectively, significant decreases in resting glucose metabolism were seen globally throughout the brain, including gray and WM structures, and regions considered relevant for maintenance of brain plasticity. Figure 2 shows an example (subject #10) of whole-body and brain PET imaging, revealing a profound decrease in global and regional brain metabolism by 44% following chemotherapy. In order to identify the potential differences in glucose metabolism among brain regions within GM, WM, and germinal zones, we applied MANOVA. GM regions were significantly more affected than WM regions ($P = 0.005$) and germinal zones ($P = 0.002$), suggesting regional differences in the effects of chemotherapy on the brain. However, even though SUV was significantly diminished in both gray and WM regions and germinal zones, no statistical difference was detected between specific subregions of GM, WM, or germinal zones.

Discussion

An increasing body of literature suggests that chemotherapy can be associated with delayed and persistent neurologic adverse effects, even in patients treated for non-CNS tumors. Commonly reported symptoms include cognitive impairment characterized by decreased attention, concentration, memory and executive function, and infrequently WM damage identified on brain imaging.[40] Despite these clinically well-recognized symptoms and findings, surprisingly little is known about the functional mechanisms underlying such adverse effects.

Using FDG-PET in combination with an advanced imaging analysis technology, we here describe the temporal and spatial pattern of platinum-based chemotherapy on resting glucose metabolism in the brain of a homogenous cohort of non-small-cell lung cancer patients treated with a comparable chemotherapy regimen. While all patients were treated with a platinum-based regimen, a contribution of other chemotherapeutic agents (e.g., Taxol, Etoposide, Alimta, Avastin, or Gemcitabine) to the findings in this study cannot be ruled out. The design of the study provided the unique opportunity to use each patient's imaging data set prior to administration of chemotherapy as an internal control for follow-up imaging during the course and after completion of chemotherapy.

Significant decreases in glucose metabolism were noted across all GM structures, including bilateral frontal, parietal and cerebellar cortices, and bilateral basal ganglia with a mean overall reduction of 22%. Decrease in resting glucose metabolism affected GM structures in both hemispheres in a comparable and overall symmetric distribution. Chemotherapy was also associated with a decrease in glucose metabolism in paraventricular and subcortical WM tracts, corpus callosum, and cerebellar WM. It

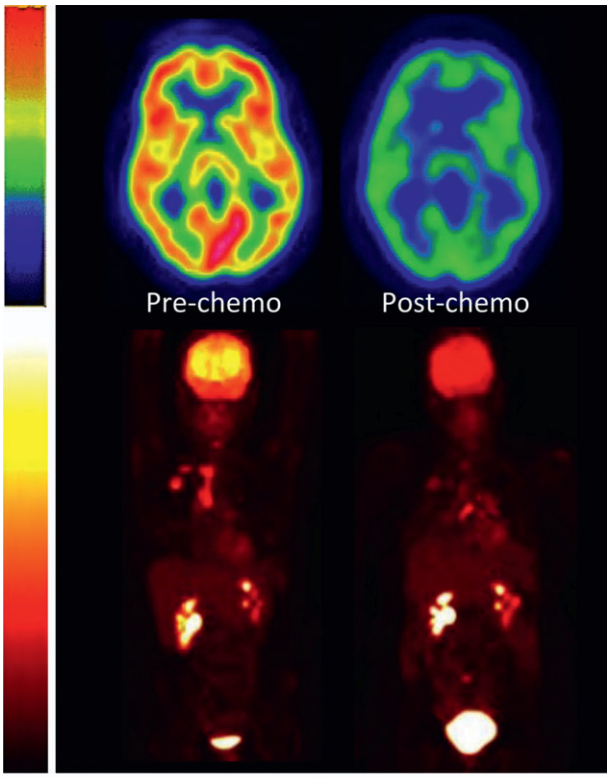

	Brain	Liver	Tumor
Pre-chemo SUV	10.0	2.3	12.2
Post-chemo SUV	5.6	2.3	9.8
% change	- 44.0	0.0	- 20.0

Figure 2. Alterations of resting state glucose metabolism prior to and after chemotherapy. Top panel: axial brain images in a representative patient (subject #10, see Table 3), demonstrating normal resting brain metabolism on the "pre-chemo" image and a reduction by 44% in the "post-chemo" image (SUV_{max} decreases from 10.0 to 5.6). In this "rainbow" color display, the areas with highest glucose metabolism are shown as orange to red. Areas with lowest glucose metabolism are shown as green to blue. Lower panel: maximum intensity projection PET images of the head through the thighs in the same patient showing the change in resting whole-body metabolism between baseline (prechemotherapy) and follow-up (post chemotherapy) imaging. In "hot lava" color display, high metabolism is indicated by yellow to white colors and low metabolism is indicated by red and black. The tumor in the right lung demonstrates a higher metabolism at baseline and lower metabolism on follow-up, compatible with a reduction in tumor size and favorable response to treatment (SUV_{max} decreases from 12.2 to 9.8, a decrease by 20%). In the liver, serving as a control organ, the values for SUV_{max} do not change between baseline and follow-up, demonstrating consistency in technique. As an additional finding on both image sets, physiologic radiotracer excretion is seen in kidneys and bladder. PET, positron emission tomography; SUV, standardized uptake value.

remains unclear, however, whether these changes were transient or might be indicative of subsequent WM changes observed by others as a consequence of chemotherapy.[22,25,30] We found that altered glucose metabolism in WM tracts was most notable in the right frontotemporal WM and corpus callosum, but overall was not significantly different between hemispheres.

To assess the impact of platinum-based chemotherapy on the germinal zones of the adult CNS, known to be highly vulnerable to chemotherapy based on preclinical studies,[38] we included bilateral hippocampi and SVZ in our analysis. Strikingly, exposure to chemotherapy resulted in a *significant* overall decrease of resting glucose metabolism by 12–13% in the bilateral SVZ. A decrease of 10–11% in glucose metabolism was also notable in bilateral hippocampi, although this change did not reach level of significance. While the biological consequences of this finding remain unknown, we speculate that significant impairment of glucose metabolism in the lateral SVZ might lend support to the current concept of the cell biological mechanisms underlying chemotherapy-associated CNS toxicity.

Collectively, GM structures appeared significantly more affected than WM and germinal zones. We were unable to identify significant differences, however, within subregions of GM, WM, or germinal zones.

To our knowledge, this represents the first functional imaging study in which quantitative changes in FDG-PET have been studied in both gray and WM structures *longitudinally* in response to chemotherapy. Our findings of differential impact of chemotherapy on brain glucose metabolism in distinct brain regions potentially offers novel insights into adverse neurologic consequences observed in cancer patients treated with chemotherapy.

We would like to point out that a potential confounding factor in our findings could be a possible change in the lumped constant (LC), defined as the conversion factor between the net uptake of FDG and glucose[43] as a consequence of chemotherapy. However, we are not aware of any data in the literature in this regard and assumed the LC to be constant over time and unaffected by systemic chemotherapy.

Our study extends the current body of literature by evaluating the effects of *platinum-based* chemotherapy in a cohort of non-small-cell lung cancer patients, whereas most other studies have focused on chemotherapy-treated breast cancer patients.[26]

We hypothesize that the integrity of germinal zones and maintenance of neural progenitor cell populations are relevant for regenerative processes following toxic insults to the CNS, and that exhaustion of progenitor cell pools in germinal zones might play an important role in long-term neurological function of cancer patients.[42]

The findings of this PET imaging study might represent a functional correlate of cell biological changes seen in preclinical studies,[38,39] by revealing metabolic changes in gray *and* WM regions, as well as in germinal zones following platinum-based chemotherapy.

To the best of our knowledge, only two other studies have used PET imaging to evaluate the impact of chemotherapy on the brain – both in breast cancer survivors and without baseline imaging prior to chemotherapy.

The first study by Silverman et al. used [O-15] H_2O and FDG-PET in breast cancer survivors treated with chemotherapy more than 5 years prior, and identified chronic GM alterations of resting glucose metabolism in fronto-cortical, cerebellar, and basal ganglia activity.[35] Impaired glucose metabolism in inferior-frontal brain regions correlated with impaired short-term memory function.[35] Using FDG-PET in breast cancer patients previously treated with chemotherapy, the same group later reported a potential correlation between circulating pro-inflammatory cytokines, cognitive complaints, and regionally impaired glucose metabolism in the medial prefrontal cortex and anterior temporal cortex.[36] Both studies were limited by the lack of imaging data prior to administration of chemotherapy, instead using non-chemotherapy-treated cancer patients as controls.

Recent functional imaging studies with fMRI have suggested that regionally altered brain function and disruption of resting state functional connectivity patterns correlate with cognitive impairment and decreased executive function in breast cancer patients treated with chemotherapy.[32–34,45]

While neurocognitive function was not formally assessed in our study, 60% of patients reported either significant memory impairment and/or mood alterations during the course of treatment, perhaps suggestive of functional neurological consequences of cancer therapy. We intend to correlate FDG-PET data with formal neuropsychological testing in future prospective studies.

It remains unclear at this point whether the observed chemotherapy effects on the brain represent acute, subacute, or delayed changes, since all follow-up FDG-PET scans were performed after a mean of four cycles of chemotherapy, corresponding to a mean time interval of 6 months between baseline and follow-up scans. At the time of follow-up PET/CT, patients were off active chemotherapy for a mean of 11 days (range 2–28 days). Therefore, the effects of chemotherapy could be the result of acute, subacute, or delayed effects. In addition, cumulative effects cannot be ruled out.

The long-term neurologic consequences of functional changes of resting glucose metabolism remain unknown. It may be noteworthy, however, that one of the subjects in our study (ID #10; Table 2) developed a marked reduction of overall brain volume after four cycles of therapy with carboplatin/taxol and subsequent bevacizumab,

as determined by an increase in ventricular volume of 20%, measured on MRI using 3DSlicer, over the course of <5 months.

It has been a daunting challenge to monitor and predict neurotoxicity in individual patients receiving chemotherapy. Despite multiple limitations, cognitive testing has been the most accessible and cost-effective approach. This study is hypothesis generating in this regard and suggests that serial FDG-PET studies of the brain might represent a potential biomarker of neurotoxicity during cancer treatment. Future prospective studies with combined PET and structural neuroimaging and longitudinal cognitive assessment might therefore offer novel mechanistic and biological insights into the vulnerability of the CNS to chemotherapy.

Collectively, this study provides novel insights into (1) changes in regional resting glucose metabolism in response to platinum-based chemotherapy in a cohort of lung cancer patients, and (2) alterations of resting metabolic activity in germinal zones (hippocampus, subventricular zone, olfactory bulb), which are areas considered relevant to endogenous CNS repair and maintenance of overall brain function. Future prospective studies combining advanced neuroimaging modalities (e.g., PET/MRI) with longitudinal assessment of neurocognitive function will allow further characterization of the long-term structural and functional consequences of chemotherapy in cancer patients, and to identify and validate the potential imaging biomarkers of neurotoxicity associated with chemotherapy.

Acknowledgments

This work was supported by the National Institute of Health (NIH) (P41 EB015898; P41 RR013218; U54 EB005149; to R. K., A. Z., and W. P.). J. Dietrich is a recipient of the American Academy of Neurology (AAN) Clinical Research Training Fellowship (CRTF). This work has also been supported by the Clinical Investigator Program (CITP) at Beth Israel Deaconess Medical Center, Harvard Medical School (to J. D.), the American Cancer Society (to J. D.), and internal funds from the Department of Radiology at BWH (to L. H.).

Conflict of Interest

Dr. Kikinis is the Principal Investigator of 3D Slicer, a software platform for single subject image analysis and visualization, used in the submitted research study.

References

1. Arrillaga-Romany I, Dietrich J. Imaging findings in cancer therapy-associated neurotoxicity. Semin Neurol 2012;32:476–486.
2. DeAngelis LM, Delattre JY, Posner JB. Radiation-induced dementia in patients cured of brain metastases. Neurology 1989;39:789–796.
3. Duffner PK. Long-term effects of radiation therapy on cognitive and endocrine function in children with leukemia and brain tumors. Neurologist 2004;10:293–310.
4. Perry A, Schmidt RE. Cancer therapy-associated CNS neuropathology: an update and review of the literature. Acta Neuropathol 2006;111:197–212.
5. Butler RW, Haser JK. Neurocognitive effects of treatment for childhood cancer. Ment Retard Dev Disabil Res Rev 2006;12:184–191.
6. Alvarez JA, Scully RE, Miller TL, et al. Long-term effects of treatments for childhood cancers. Curr Opin Pediatr 2007;19:23–31.
7. van Dam FS, Schagen SB, Muller MJ, et al. Impairment of cognitive function in women receiving adjuvant treatment for high-risk breast cancer: high-dose versus standard-dose chemotherapy. J Natl Cancer Inst 1998;90:210–218.
8. Schagen SB, van Dam FS, Muller MJ, et al. Cognitive deficits after postoperative adjuvant chemotherapy for breast carcinoma. Cancer 1999;85:640–650.
9. Brezden CB, Phillips KA, Abdolell M, et al. Cognitive function in breast cancer patients receiving adjuvant chemotherapy. J Clin Oncol 2000;18:2695–2701.
10. Ahles TA, Saykin A. Cognitive effects of standard-dose chemotherapy in patients with cancer. Cancer Invest 2001;19:812–820.
11. Schagen SB, Muller MJ, Boogerd W, et al. Late effects of adjuvant chemotherapy on cognitive function: a follow-up study in breast cancer patients. Ann Oncol 2002;13:1387–1397.
12. Wefel JS, Lenzi R, Theriault RL, et al. The cognitive sequelae of standard-dose adjuvant chemotherapy in women with breast carcinoma: results of a prospective, randomized, longitudinal trial. Cancer 2004;100:2292–2299.
13. Schagen SB, Muller MJ, Boogerd W, et al. Change in cognitive function after chemotherapy: a prospective longitudinal study in breast cancer patients. J Natl Cancer Inst 2006;98:1742–1745.
14. Hurria A, Rosen C, Hudis C, et al. Cognitive function of older patients receiving adjuvant chemotherapy for breast cancer: a pilot prospective longitudinal study. J Am Geriatr Soc 2006;54:925–931.
15. Ahles TA, Saykin AJ. Candidate mechanisms for chemotherapy-induced cognitive changes. Nat Rev Cancer 2007;7:192–201.
16. Vardy J, Rourke S, Tannock IF. Evaluation of cognitive function associated with chemotherapy: a review of published studies and recommendations for future research. J Clin Oncol 2007;25:2455–2463.
17. Hermelink K. Acute and late onset cognitive dysfunction associated with chemotherapy in women with breast cancer. Cancer 2011;117:1103, author reply 1103–1104.

18. Wefel JS, Saleeba AK, Buzdar AU, et al. Acute and late onset cognitive dysfunction associated with chemotherapy in women with breast cancer. Cancer 2010;116:3348–3356.
19. Wefel JS, Schagen SB. Chemotherapy-related cognitive dysfunction. Curr Neurol Neurosci Rep 2012;12:267–275.
20. Hutchinson AD, Hosking JR, Kichenadasse G, et al. Objective and subjective cognitive impairment following chemotherapy for cancer: a systematic review. Cancer Treat Rev 2012;38:926–934.
21. Koppelmans V, Breteler MM, Boogerd W, et al. Neuropsychological performance in survivors of breast cancer more than 20 years after adjuvant chemotherapy. J Clin Oncol 2012;30:1080–1086.
22. Deprez S, Amant F, Smeets A, et al. Longitudinal assessment of chemotherapy-induced structural changes in cerebral white matter and its correlation with impaired cognitive functioning. J Clin Oncol 2012;30:274–281.
23. Koppelmans V, de Ruiter MB, van der Lijn F, et al. Global and focal brain volume in long-term breast cancer survivors exposed to adjuvant chemotherapy. Breast Cancer Res Treat 2012;132:1099–1106.
24. McDonald BC, Conroy SK, Ahles TA, et al. Alterations in brain activation during working memory processing associated with breast cancer and treatment: a prospective functional magnetic resonance imaging study. J Clin Oncol 2012;30:2500–2508.
25. de Ruiter MB, Reneman L, Boogerd W, et al. Late effects of high-dose adjuvant chemotherapy on white and gray matter in breast cancer survivors: converging results from multimodal magnetic resonance imaging. Hum Brain Mapp 2012;33:2971–2983.
26. Kaiser J, Bledowski C, Dietrich J. Neural correlates of chemotherapy-related cognitive impairment. Cortex 2014;54C:33–50.
27. Inagaki M, Yoshikawa E, Matsuoka Y, et al. Smaller regional volumes of brain gray and white matter demonstrated in breast cancer survivors exposed to adjuvant chemotherapy. Cancer 2007;109:146–156.
28. Koppelmans V, Schagen SB, Poels MM, et al. Incidental findings on brain magnetic resonance imaging in long-term survivors of breast cancer treated with adjuvant chemotherapy. Eur J Cancer 2011;47:2531–2536.
29. McDonald BC, Conroy SK, Ahles TA, et al. Gray matter reduction associated with systemic chemotherapy for breast cancer: a prospective MRI study. Breast Cancer Res Treat 2010;123:819–828.
30. Abraham J, Haut MW, Moran MT, et al. Adjuvant chemotherapy for breast cancer: effects on cerebral white matter seen in diffusion tensor imaging. Clin Breast Cancer 2008;8:88–91.
31. de Ruiter MB, Reneman L, Boogerd W, et al. Cerebral hyporesponsiveness and cognitive impairment 10 years after chemotherapy for breast cancer. Hum Brain Mapp 2011;32:1206–1219.
32. Ferguson RJ, McDonald BC, Saykin AJ, et al. Brain structure and function differences in monozygotic twins: possible effects of breast cancer chemotherapy. J Clin Oncol 2007;25:3866–3870.
33. Kesler SR, Bennett FC, Mahaffey ML, et al. Regional brain activation during verbal declarative memory in metastatic breast cancer. Clin Cancer Res 2009;15:6665–6673.
34. Kesler SR, Kent JS, O'Hara R. Prefrontal cortex and executive function impairments in primary breast cancer. Arch Neurol 2011;68:1447–1453.
35. Silverman DH, Dy CJ, Castellon SA, et al. Altered frontocortical, cerebellar, and basal ganglia activity in adjuvant-treated breast cancer survivors 5–10 years after chemotherapy. Breast Cancer Res Treat 2007;103: 303–311.
36. Pomykala KL, Ganz PA, Bower JE, et al. The association between pro-inflammatory cytokines, regional cerebral metabolism, and cognitive complaints following adjuvant chemotherapy for breast cancer. Brain Imaging Behav 2013;7:511–523.
37. Seigers R, Schagen SB, Van Tellingen O, et al. Chemotherapy-related cognitive dysfunction: current animal studies and future directions. Brain Imaging Behav 2013;7:453–459.
38. Dietrich J, Han R, Yang Y, et al. CNS progenitor cells and oligodendrocytes are targets of chemotherapeutic agents in vitro and in vivo. J Biol 2006;5:22.
39. Han R, Yang YM, Dietrich J, et al. Systemic 5-fluorouracil treatment causes a syndrome of delayed myelin destruction in the central nervous system. J Biol 2008;7:12.
40. Dietrich J, Monje M, Wefel J, et al. Clinical patterns and biological correlates of cognitive dysfunction associated with cancer therapy. Oncologist 2008;13:1285–1295.
41. Hyrien O, Dietrich J, Noble M. Mathematical and experimental approaches to identify and predict the effects of chemotherapy on neuroglial precursors. Cancer Res 2010;70:10051–10059.
42. Monje M, Dietrich J. Cognitive side effects of cancer therapy demonstrate a functional role for adult neurogenesis. Behav Brain Res 2012;227:376–379.
43. Reivich M, Alavi A, Wolf A, et al. Glucose metabolic rate kinetic model parameter determination in humans: the lumped constants and rate constants for [18F] fluorodeoxyglucose and [11C]deoxyglucose. J Cereb Blood Flow Metab 1985;5:179–192.
44. Fedorov A, Beichel R, Kalpathy-Cramer J, et al. 3D Slicer as an image computing platform for the Quantitative Imaging Network. Magn Reson Imaging 2012;30: 1323–1341.
45. Kesler SR, Wefel JS, Hosseini SM, et al. Default mode network connectivity distinguishes chemotherapy-treated breast cancer survivors from controls. Proc Natl Acad Sci USA 2013;110:11600–11605.

